

# NUMERICAL AND THEORETICAL INVESTIGATION OF HELICOPTER DITCHING WITH VARIOUS INITIAL VELOCITY AND PITCHING ANGLE

Li Zheng<sup>1</sup>, Mingyi Wang<sup>2</sup>, Yujin Lu<sup>2</sup>, Hongyu Qiao<sup>1</sup>, Tianhang Xiao<sup>1</sup> & Shuanghou Deng<sup>1</sup>

<sup>1</sup>Nanjing University of Aeronautics and Astronautics, Nanjing, 210016, People's Republic of China <sup>2</sup>Chinese Aeronautical Establishment, Beijing, 100012, People's Republic of China

#### **Abstract**

The dynamic behaviors of helicopter resulting from the varying initial downward velocity and pitching angle have been analyzed numerically and theoretically in the present study during water impacting. The air-water two phase flows are computed by solving unsteady Reynolds-Averaged Navier-Stokes equations enclosed by standard k-omega turbulence model. A treatment for computational domain in combination with a global dynamic mesh technique is applied to deal with the relative motion between the helicopter and water. Results demonstrate the effects of initial downward velocity and pitching angle on the ditching process in detail. A shape factor and an average deadrise angle are introduced to extend the theoretical model for predicting the kinematic parameters during ditching.

**Keywords:** helicopter, ditching, dynamic mesh, theoretical model

## 1. Introduction

On account of the limited resource on the inland area, great attention and interest have been gained on the exploration of ocean resource by a large quantity of researchers and governments. In order to complete the mission efficiently above the sea, flight vehicles, such as amphibious aircraft, helicopter, wing-in-ground craft (WIG), etc., have been widely employed for transportation and the main operational time occurs over the water which can be a reason for the investigation of emergency landing on water, generally called ditching. Besides, differing from impacting on hard surface, it experiences more significant circumstances, including over-pressure, air cushion, cavitation and suction, etc. [1]. A wide range of parameters that affect the performance of dynamic behavior, when a flight vehicle ditches on water, has been discussed by a great deal of scientists and institutions for a long time. The generic aircraft, reported by NACA TN2929, was investigated with respect to the effect of rearfuselage shape, such as changes in longitudinal curvatures, the cross section and fuselage fineness ratio, on ditching behavior through experimental study [2] and computational simulation [3]. The conclusion deduced from the work is the minimum longitudinal curvature and circular cross section are most suitable for high landing speed while moderate longitudinal curvature with moderately curved cross section is desirable for the lower speed. Also, the higher fineness ratio will make the safer ditching process. Subsequently, the focus of aircraft ditching behavior alternated on the study of the effects of aerodynamic configurations, including wing, horizontal tail and flaps, using the finite volume method coupled with the volume of fluid model [3], as well as the role of the aerodynamic loads. It also suggested that a significant manner is influenced by the aerodynamic load, through the comparisons of dynamic behavior on the pure fuselage, wing-body combination, wing-body-horizontal tail combination and the complete configuration with deflected flaps which results in the smaller nose-up moment and the smaller maximum attitude. The effect of the initial pitch angle on the ditching performance of a civil aircraft model consisting of low-mid wing and low horizontal tail was demonstrated numerically by Guo et al. [4]. It indicated that the initial pitch angle has significant effect on the normal load, except for the maximum longitudinal load and maximum pressure on the fuselage. To

reduce the load, an incident angle between 10 and 12deg has been proposed as a recommendation for the aircraft ditching with similar configuration. The ditching of a WIG ship under different velocity components with the attack angle unchanged was simulated by Cheng et al. [5] using a smoothed particle hydrodynamics (SPH) method. And it concluded that the maximum impacting acceleration occurs during the first sliding stage and is mainly influenced by the vertical velocity rather than the horizontal velocity in the regulation the acceleration increases with the augment of the vertical velocity significantly.

However, a few direct investigations on ditching behaviors connecting with theoretical estimation have been presented. At this point, the main objective of this paper is to establish the essential comprehension and evaluation of ditching characteristics from the view of initial condition, such as downward velocity and pitching angle. A three-dimensional helicopter scaled model was chosen as the object of study, ditching on still water. This paper is organized as follows: the theoretical and numerical methods are introduced in Section 2. Section 3 subsequently presents the simulation and the analysis of the helicopter ditching with conclusions drawn in Section 4.

# 2. Methodology and Computational Setup

## 2.1 Theoretical Estimation

Based on the extended von Karman's theory [6] for wedge impacting scenario (see Figure 1), it is possible to compute the maximal impact acceleration and the corresponding penetration depth, velocity and time when acceleration reaches its peak value:

$$a_{z\max} = v_{z0}^2 \left(\frac{5}{6}\right)^3 \frac{\gamma}{\tan(\beta)} \sqrt{\frac{2\pi\rho}{5M}}$$
 (1a)

$$z^* = \sqrt{\frac{2M}{5\pi\rho\gamma^2}}\tan(\beta) \tag{1b}$$

$$v_z^* = \frac{5}{6}v_{z0} \tag{1c}$$

$$t^* = \frac{1}{v_{z0}} \frac{16}{15} \sqrt{\frac{2M}{5\pi\rho\gamma^2}} \tan(\beta)$$
 (1d)

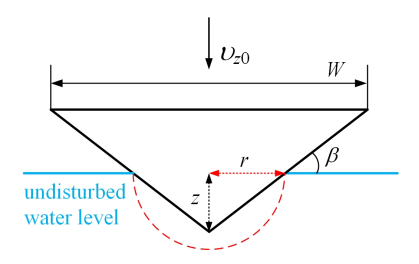


Figure 1 – Wedge water entry scenario.

For helicopter ditching event, the corresponding definition of the deadrise angle  $\beta$ , pile-up coefficient  $\gamma$  and mass M is not clear. Thus, the formula of maximal acceleration can be written as:

$$a_{\text{zmax}} = \left(\frac{5}{6}\right)^3 \sqrt{\frac{2\pi\rho}{5}} \cdot S(\gamma, \beta, M) \cdot v_{z0}^2 \tag{2}$$

where  $S(\gamma, \beta, M)$  is shape factor.

Then, the corresponding penetration depth  $z^*$  and time  $t^*$  can be expressed by the shape factor:

$$z^* = \mu_{3D} \cdot \sqrt{\frac{2}{5\pi\rho}} \cdot \frac{1}{S(\gamma,\beta,M)}$$
 (3)

$$t^* = \mu_{3D} \cdot \frac{1}{v_{z0}} \frac{16}{15} \sqrt{\frac{2}{5\pi\rho}} \cdot \frac{1}{S(\gamma, \beta, M)}$$
 (4)

where  $\mu_{3D}$  is three-dimension factor and equals to 2/3.

#### 2.2 Numerical Method

In the present study the unsteady incompressible Reynolds-averaged Navier-Stokes equations with a standard  $k-\omega$  two-equation turbulence model are solved by the finite volume method. The governing equations for the continuity condition and the momentum conservation condition can be written as:

$$\frac{\partial u_i}{\partial x_i} = 0 \tag{5}$$

$$\rho \frac{\partial u_i}{\partial t} + \rho \frac{\partial}{\partial x_i} (u_i u_j) = -\frac{\partial p}{\partial x_i} + \frac{\partial}{\partial x_i} (v \frac{\partial u_i}{\partial x_i} - \rho \overline{u_i' u_j'}) + \rho g_i$$
 (6)

where  $u_i$  and  $u_j$  (i, j = 1,2,3) are the time averaged value of velocity,  $x_i$  and  $x_j$  (i, j = 1,2,3) are the spatial coordinate components,  $\rho$  is the fluid density, p is the fluid pressure, v is the fluid kinematic viscosity,  $-\rho \overline{u_i'u_j'}$  is the Reynolds stress, and  $g_i$  is the gravitational acceleration in the i-th direction. The Semi-Implicit Pressure Linked Equations (SIMPLE) algorithm is employed to achieve an implicit coupling between pressure and velocity, and the gradient is reconstructed with the Green-Gauss Node Based method. The modified High Resolution Interface Capturing (HRIC) scheme is adopted for volume fraction transport. The convection terms, as well as the diffusion terms, are turned into algebraic parameters using second-order upwind and second-order central methods, respectively. The unsteady terms are discretized in the time domain by applying a second-order implicit scheme. Volume of fluid (VOF) scheme, originally proposed by [7], is used in the present computational scheme to capture the water-air interface by introducing a variable,  $\alpha_w$ , called the volume fraction of the water in the computational cell, which varies between 0 (air) and 1 (water) and is defined as:

$$\alpha_{\rm w} = V_{\rm w}/V,\tag{7}$$

where  $V_{\rm w}$  is the volume of water in the cell and V is the volume of the cell. The volume fraction of the air in a cell can be computed as:

$$\alpha_{\rm a} = 1 - \alpha_{\rm w}. \tag{8}$$

The volume of fraction is governed by the following equation:

$$\frac{\partial \alpha}{\partial t} + u_i \frac{\partial \alpha}{\partial x_i} = 0. \tag{9}$$

The effective value  $\varphi_m$  of any physical properties, such as density, viscosity, etc., of the mixture of water and air in the transport equations is determined by:

$$\varphi_{\rm m} = \varphi_{\rm w} \alpha_{\rm w} + \varphi_{\rm a} (1 - \alpha_{\rm w}). \tag{10}$$

To accurately capture the dynamic behavior and the load generated by the water-entry process, the motion of the body caused by the fluid forces and moments at the surface is determined via a six degree-of-freedom (6DOF) model. The 6DOF model solves the equations for the rotation and translation of the center of mass of the object. The equation for the translation is formulated in the global inertial coordinate system:

$$M \cdot \frac{\mathrm{d}v}{\mathrm{d}t} = F,\tag{11}$$

and the rotation of the object is solved in the body local coordinate system by:

$$L\frac{\mathrm{d}\omega}{\mathrm{d}t} + \omega \times L\omega = M. \tag{12}$$

Subsequently, a dynamic mesh strategy [8], which moves the entire mesh rigidly along with the object at each time step according to the solution of the 6DOF model, is employed to deal with the relative motion between the fluid and the rigid body with on single grid domain. The detailed description about the mesh method can be found in our previous study [6].

## 3. Results and Discussion

Figure 2 presents the initial flow field of helicopter ditching on still water. In the present study, the helicopter performs a three-degree-of-freedom landing motion (pitch, horizontal, and vertical displacement), ignoring the lift of rotor during this process. To conserve computational resources, the numerical simulation is conducted using a half model. Furthermore, to simplify the model, the impacts of the rotor and other components are not considered. Detailed size parameters of the helicopter model are listed in Table 1.

The dimension of the computational domain and the boundary conditions for the helicopter ditching scenario are also highlighted in Figure 2. The computational domain adopts a rectangular configuration with dimensions: length 4L, width L, and height 3L. Given the high orthogonality of the Cartesian grid, it is better suited to capture the free surface. Therefore, in this case, the entire computational domain is divided using a Cartesian grid. The grid is separately refined in the vicinity of the body and the front area and the total number of grid is approximately 10 million.

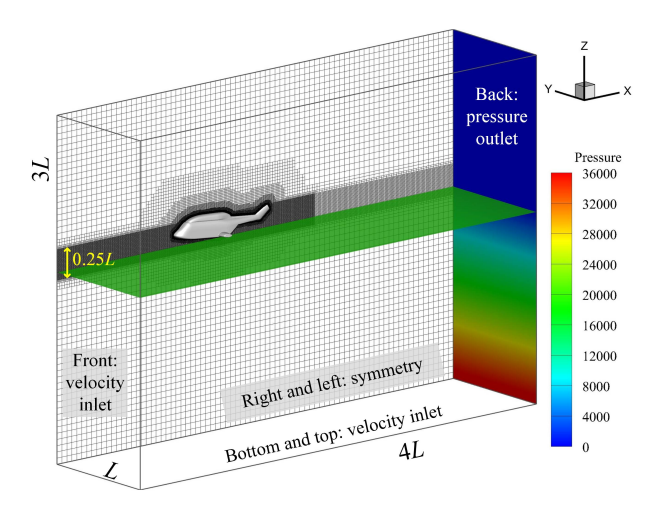


Figure 2 – Computational domain and boundary conditions.

Table 1 – Parameters of the helicopter model.

parameter	value		
fuselage length $L$ , m	2.4		
fuselage width $W$ , m	0.574		
mass $M$ , kg	25.39		
$I_{xx}, I_{yy}, I_{zz}, \text{ kg} \cdot \text{m}^2$	1.21, 4.58, 0.46		
forward and downward speed, m/s	5, 0.5		

## 3.1 Effect of Initial Downward Velocity

Firstly, the effect of initial downward velocity on hydrodynamic characteristics of helicopter ditching is discussed. Note that the initial pitch angle of the helicopter  $\theta_0 = 6^{\circ}$ , and the initial downward velocity  $v_{z0}$  under consideration are 1, 1.5, 2, 2.5, 3, 3.5, and 4 m/s. In the real situation, the variation range of water landing velocity is relatively small. In order to discuss the validity of the theoretical relationship, the range of  $v_{z0}$  during simulation is relatively large.

The comparison of vertical acceleration  $a_z$  for different  $v_{z0}$  is presented in Figure 3a. Due to the presence of small wings on both sides of the helicopter, the acceleration is slightly different at the early stage, but the overall trend still conforms to the law of free water entry motion. It can be seen that  $a_z$  increases with  $v_{z0}$  and reaches its peak in a shorter time. Then, the peak vertical acceleration  $a_{zmax}$  is extracted from Figure 3a and associated with  $v_{z0}$ , as shown in Figure 3b. It is worth noting that  $a_{zmax}$  is still a linear function of the square of the initial downward velocity  $v_{z0}^2$ , expressed as  $a_{zmax} = 10.0841v_{z0}^2 - 1.5655$ . Combining the theoretical relationship (2) mentioned in

Section 2.1( $a_{zmax} = (5/6)^3 \sqrt{2\pi\rho/5} \cdot S(\gamma, \beta, M) \cdot v_{z0}^2$ ), the shape factor  $S(\gamma, \beta, M) = 4.1311$  is obtained, which will be used in the following discussion for other kinematic parameters.

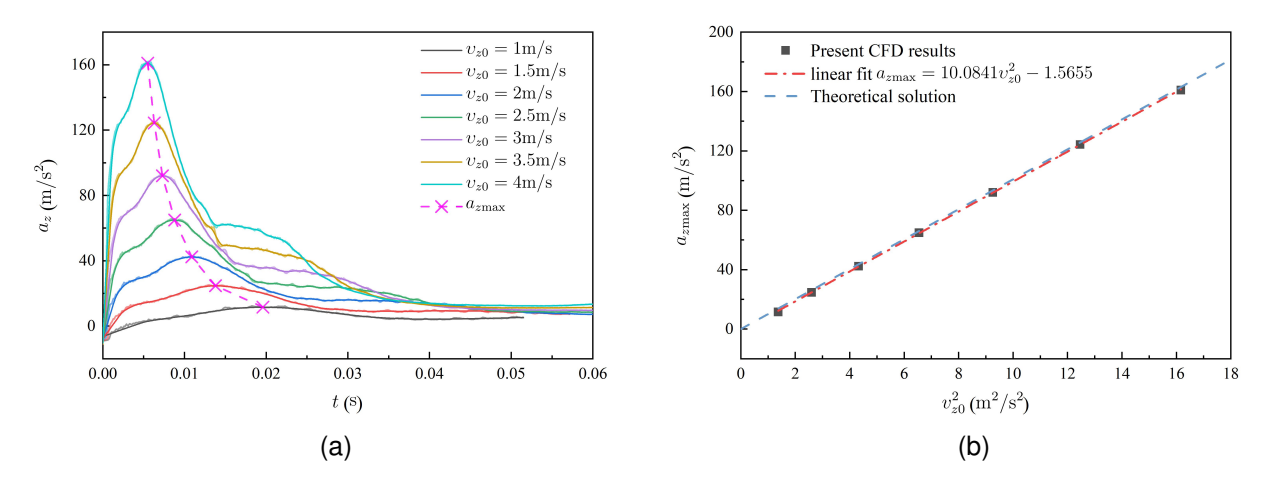


Figure 3 – Effect of initial downward velocity on vertical acceleration for helicopter ditching with  $\theta_0 = 6^\circ$ : (a) time histories of  $a_z$ ; (b) relationship between  $a_{zmax}$  and  $v_{z0}$ .

Figure 4 shows the effect of the initial downward velocity on other kinematic parameters  $(t^*, z^*, \theta, v_x^*, v_z^*, and \kappa)$  when maximum vertical acceleration is achieved. In Figure 4a, it can be found that the corresponding time  $t^*$  is a linear function of  $v_{z0}^{-1}$ . In addition, substituting the shape factor  $S(\gamma, \beta, M) = 4.1311$  into equation (4)  $(t^* = 16\sqrt{2/5\pi\rho}/(15v_{z0}S(\gamma, \beta, M)))$ , temporarily ignoring the three-dimension factor  $\mu_{\rm 3D}$ ), the expression of  $t^*$  is obtained,  $t^* = 0.0245v_{z0}$ . Compared with the numerical results, as shown in Figure 4a, the theoretical solution is in good agreement with the numerical results, and the error  $\mu$  is less than 10%. It is worth noting that herein the three-dimensional effect is not considered, the accuracy of the theoretical solution is already very high, indicating that the three-dimensional effect is weak under the current condition. The main reason is that the bottom surface of the helicopter is relatively flat along the transverse direction, which weakens the three-dimensional effect brought by the span-wise fluid flow.

Observing the corresponding penetration depth  $z^*$  in Figure 4b, it can be found that as  $v_{z0}$  increases,  $z^*$  shows a gradually decreasing trend and approaches to a constant value. Particularly, in the case of small  $v_{z0}$ , the gravity effect can be observed, that is similar to the finding in the work of Lu et al. [6]. Substituting the shape factor  $S(\gamma, \beta, M) = 4.1311$  into equation (3)  $(z^* = \sqrt{2}/5\pi\rho/S(\gamma, \beta, M))$ , ignoring the three-dimensional effect  $\mu_{3D}$ ), the corresponding penetration depth  $z_{\text{theory}}^* = 0.0229$  is obtained, which is slightly different from the present numerical results in Figure 4b. If the three-dimension factor,  $\mu_{3D}=0.9442$  concluded from  $t^*$ , is considered herein, a correction value  $\mu_{3D}\cdot z^*_{theory}=0.0216$  is obtained, which is closer to the numerical results, while there is still a slight difference. In general, the prediction accuracy of  $z^*$  using the theoretical formula (3) is sufficient with error lower than 10%. Another parameter describing the ditching performance of the helicopter, the corresponding downward velocity  $v_z^*$ , is shown in Figure 4c. It can be seen that  $v_z^*$  has a linear relationship with the initial downward velocity  $v_{z0}$ ,  $v_z^* = 0.8027v_{z0} + 0.1041$ . Since the theoretical relation of these two parameters is not affected by the shape parameters, the theoretical solution  $v_z^* = 5v_{z0}/6$  is represented by a blue dashed line in Figure 4c. It can be observed that the theoretical solution has a high degree of coincidence with the numerical results. The change of  $\kappa$ , as shown in Figure 4d, can be further used to explore this linear relationship. As  $v_{z0}$  increases, the value of  $\kappa$  gradually decreases, and when  $v_{z0}$  is greater than 2.5 m/s,  $\kappa$  gradually approaches the theoretical value 5/6. It is worth noting that at small initial downward velocity, the numerical results of  $\kappa$  and  $z^*$  are significantly deviated from the respective approaching values, indicating that the gravity effect encountered in the two-dimensional situation [6] also exists in the case of the three-dimensional helicopter ditching with small velocity. Furthermore, the comparison of variation of pitching angle  $\theta$  for different  $v_{z0}$  cases is shown in Figure 5a. It can be observed that the pitching angle of helicopter shows a trend of first decreasing and then increasing after touching the water. The pitch angle decreases first because the initial water

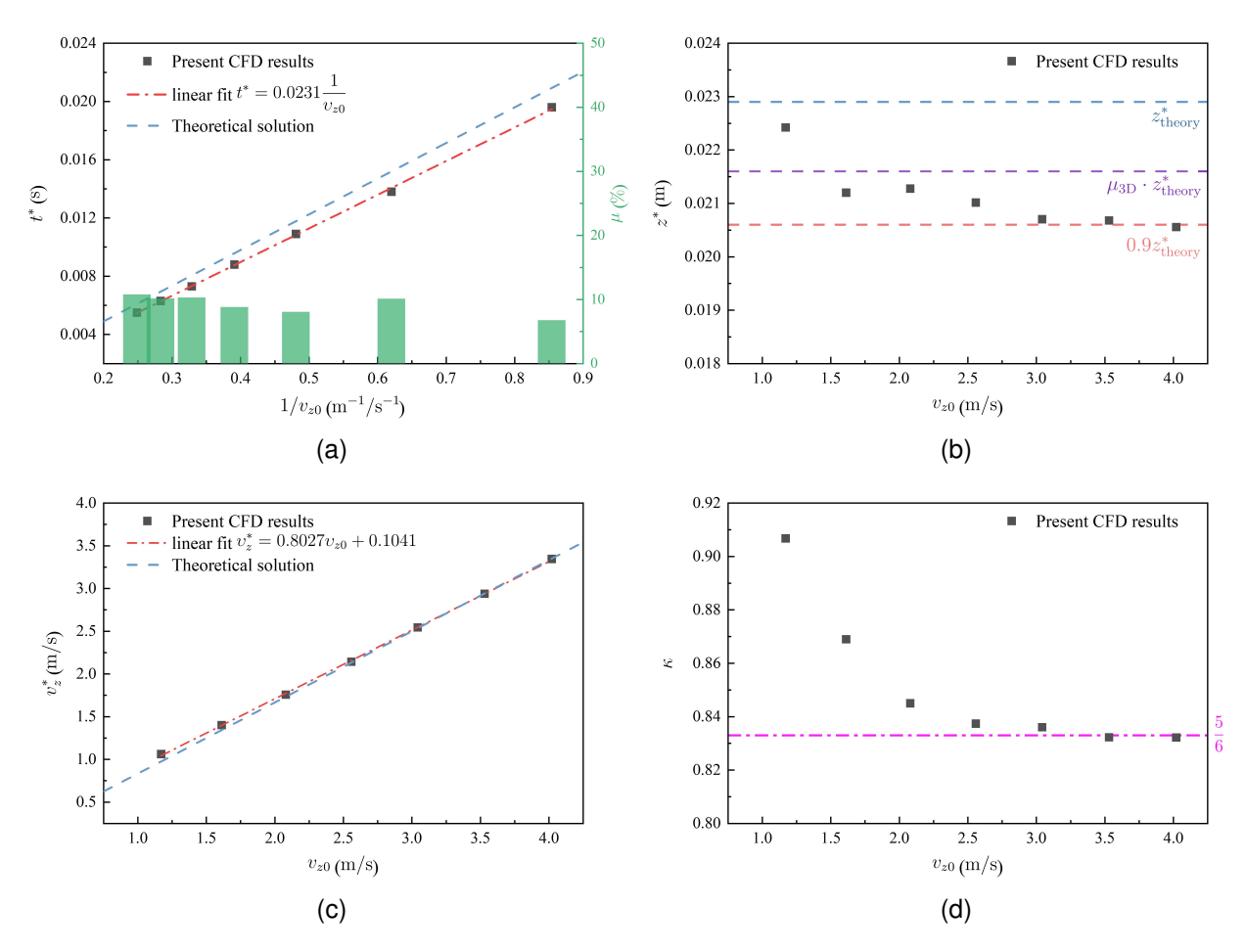


Figure 4 – Effect of initial downward velocity on variable dynamic parameters for helicopter ditching with  $\theta_0 = 6^\circ$ : (a)  $t^*$ ; (b)  $z^*$ ; (c)  $v_z^*$ ; (d)  $\kappa$ .

landing point of the body is behind the center of gravity. Due to the fluid force and gravity, a negative angular acceleration is generated, as shown in Figure 5b. Combining Figure 5a and Figure 5c, it can be known that when the  $a_z$  reaches the maximum value, the corresponding pitching angle and horizontal velocity for all cases are almost same, only the corresponding downward velocity  $v_z^*$  is different (see Figure 4c).

Pressure distribution and water deformation for different initial downward velocity of helicopter when  $a_z$  reaches its maximum are presented in Figure 6, where the pressure coefficient  $C_p$  is defined as  $C_p = (p-p_0)/(0.5\rho v_{x0}^2)$ . Note that  $v_x^*$  for all cases is relatively small, thus  $v_{x0}$  is used herein. As it can be seen that the small wing on the two sides of the body participates in the ditching process, which can provide the static buoyancy in the case of a small draft. It can also be used to explain the slight differences between the numerical and theoretical results on  $z^*$  (see Figure 4b). In addition, comparing Figure 6a and Figure 6f, some bubbles are generated at the bottom of the body when ditching at high velocity, while facing low velocity it is not obvious. It is worth noting that, although the pressure coefficient on the bottom surface of the fuselage is different in magnitude on different conditions, a similar phenomenon can be observed on the pressure distribution for all cases, that is a over-pressure appeared in the front area and a negative pressure formed in the rear area. Due to the existence of the negative pressure zone, the angular acceleration  $\dot{\omega}_y$  gradually increases (see Figure 5b), resulting in the increase of pitching angle of the helicopter. It also explains the change of the first decreasing and then increasing pitching angle described in Figure 5a.

To have a further understanding of the negative pressure, downward and horizontal velocity distribution on longitudinal section for different initial downward velocity of helicopter when  $a_z$  reaches its maximum are presented in Figure 7 and Figure 8 respectively. Note that both the downward and horizontal velocity are dimensionless, referring to the initial downward and horizontal velocity of each

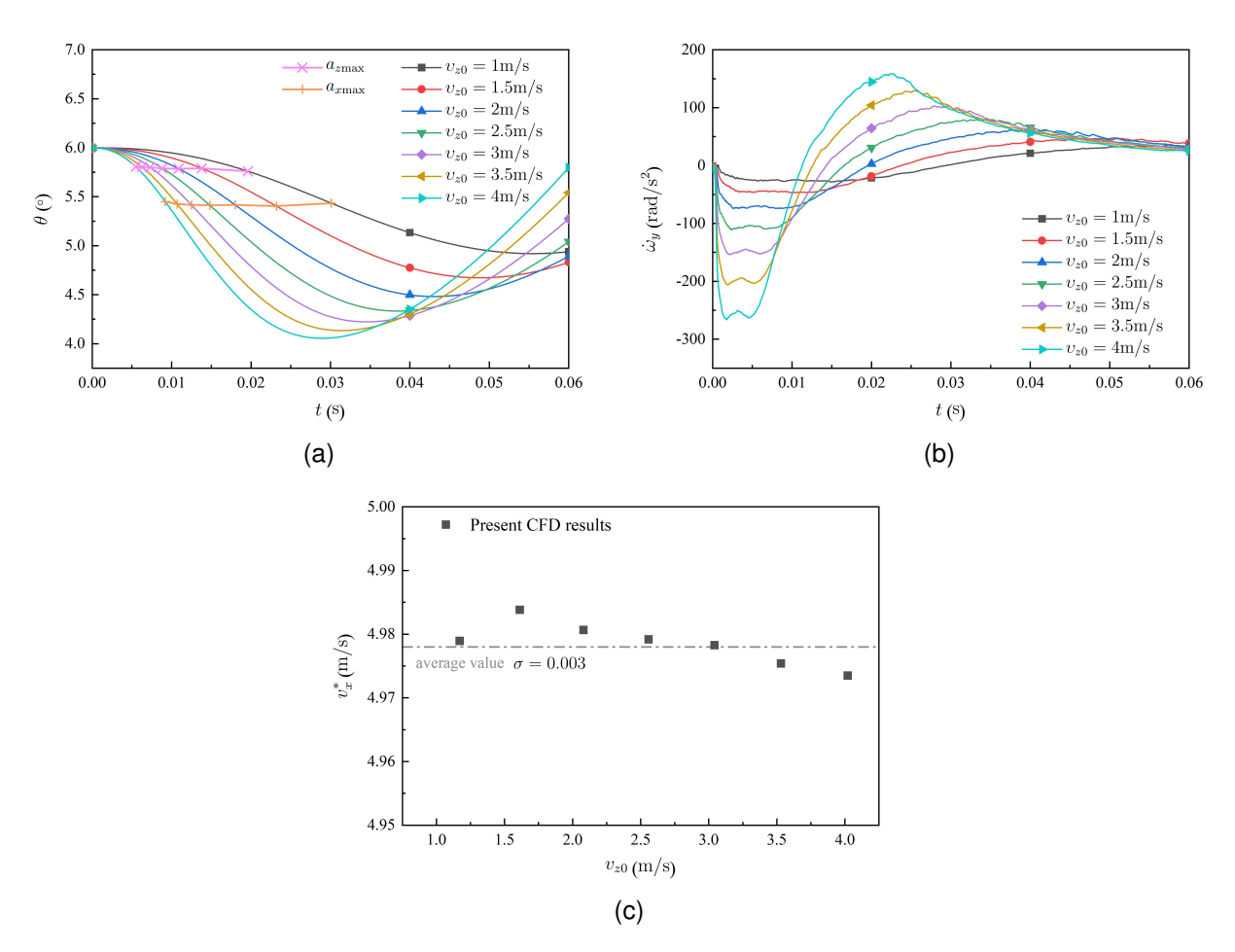


Figure 5 – Effect of initial downward velocity on pitching angle and horizontal velocity for helicopter ditching with  $\theta_0 = 6^{\circ}$ : (a) time histories of  $\theta$ ; (b)  $\dot{\omega}_v$ ; (c)  $v_x^*$ .

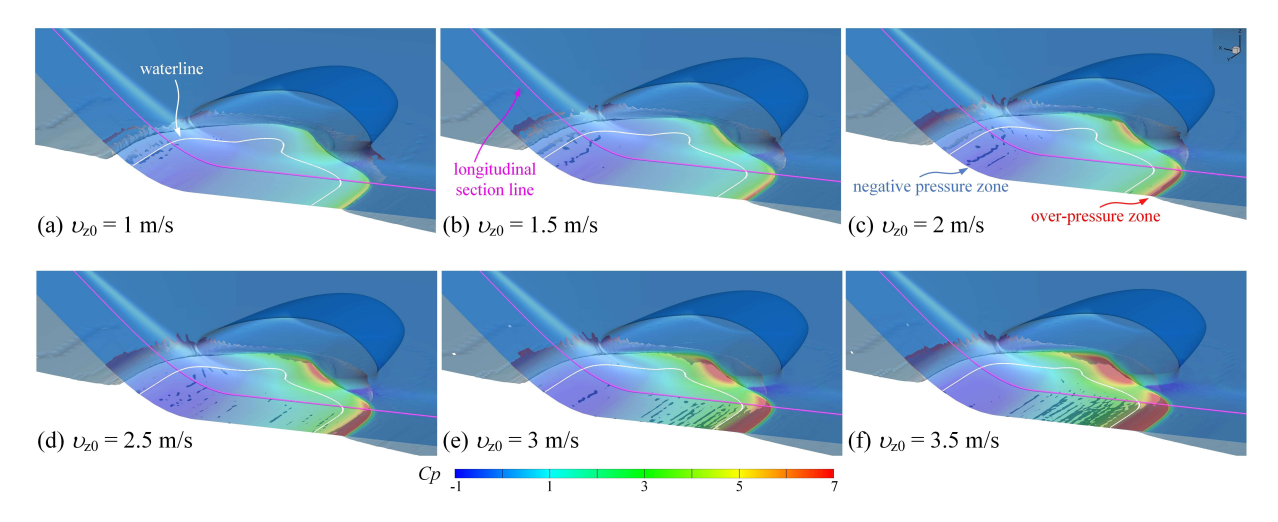


Figure 6 – Pressure distribution and water deformation for different initial downward velocity of helicopter when  $a_z$  reaches its maximum

# condition.

In terms of downward velocity distribution, due to the motion of the fuselage, the fluid below the bottom surface of the fuselage obtains a body-following downward velocity, while the fluid on both sides moves along the object surface. At this moment, the body can be regarded as an asymmetric wedge entering the water. Since the angle between the object surface and the free surface on the left side is larger than the right side, the fluid tends to move upward along the left side surface, especially in the water entry of the asymmetric wedge with horizontal velocity. In addition, from the magnitude

and distribution of downward velocity, the color with smaller velocity condition is darker, indicating that the ratio  $v_z/v_{z0}$  is larger, while in the case of larger velocity (such as Figure 7d, e and f), the distribution of downward velocity is almost same, which is consistent with the change of  $\kappa$  shown in Figure 4d.

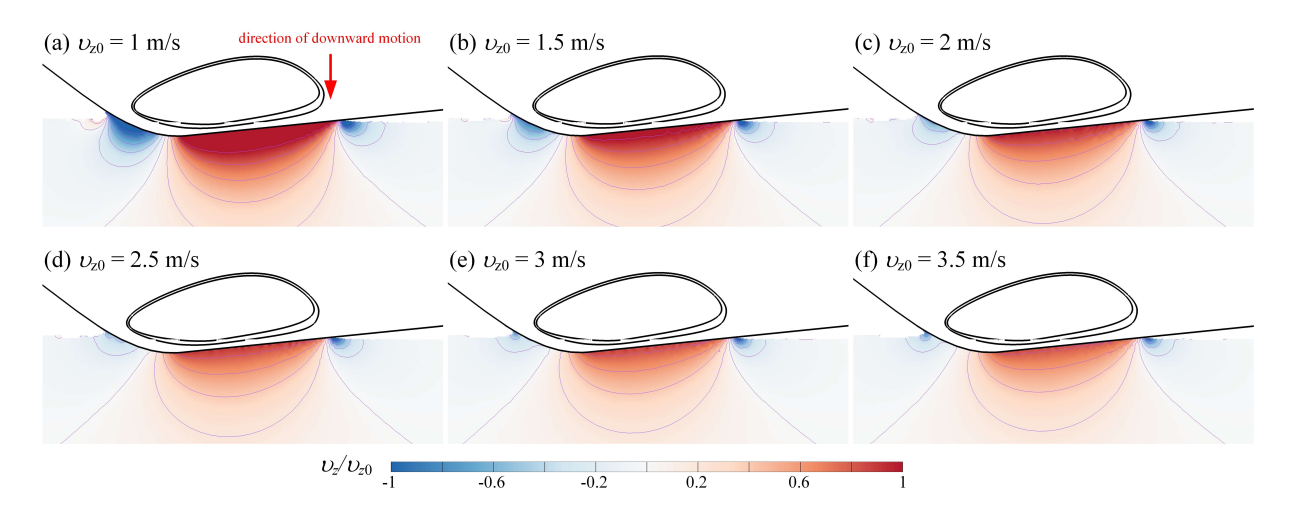


Figure 7 – Downward velocity distribution on longitudinal section for different initial downward velocity of helicopter when  $a_z$  reaches its maximum

Moving to horizontal velocity distribution (see Figure 8), the direction of horizontal motion points to the right side. A similar phenomenon can be observed on the fluid which is in the front part of the bottom surface of the fuselage, consistent with the flat plate ditching scenario [9]. However, in the rear area, due to the upward contraction of the longitudinal section line of the fuselage, the nearby fluid obtains more development space and quickly escapes in the opposite direction to the body motion, generating a larger relative velocity compared with the velocity of fuselage. In general, a larger relative motion velocity in both vertical velocity and horizontal velocity is generated near the rear part, while the front area only exists relative velocity in terms of vertical velocity. It can be concluded that the formation of the negative pressure area is mainly related to the relative motion of the fluid and the object, that is, a larger relative velocity is more likely to generate a negative pressure area. For the helicopter ditching event, the negative pressure is mainly concentrated in the area where the fuselage longitudinal section curve changes drastically. Therefore, reasonable control of the fuselage longitudinal section curve can effectively suppress or utilize the negative pressure area.

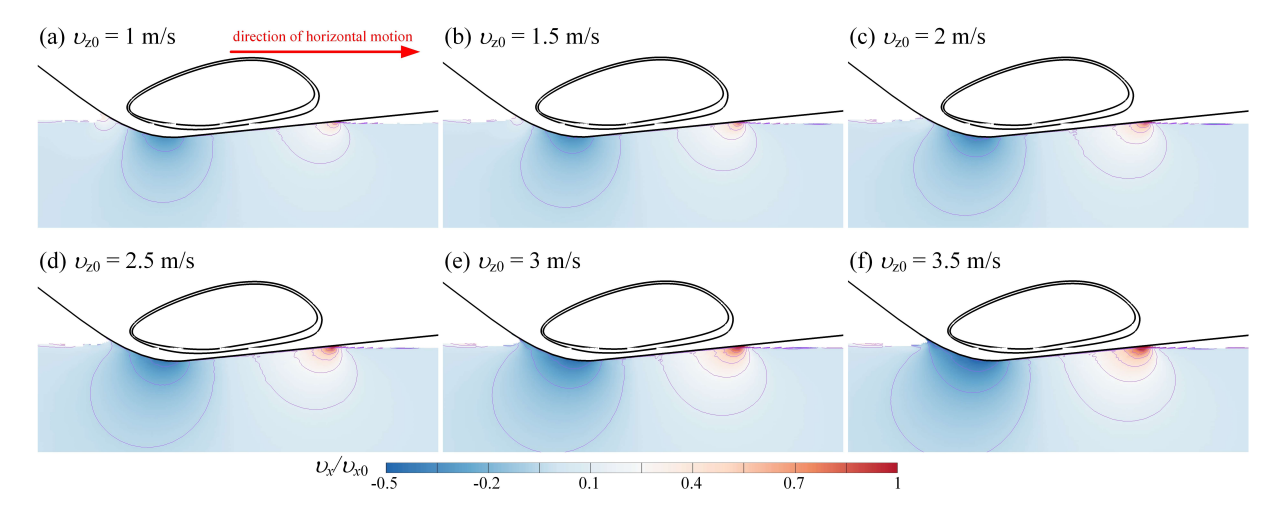


Figure 8 – Horizontal velocity distribution on longitudinal section for different initial downward velocity of helicopter when  $a_z$  reaches its maximum

Due to the helicopter ditching with an initial horizontal velocity, it is necessary to further discuss the

horizontal acceleration  $a_x$ . Time histories of  $a_x$  from different cases of  $v_{z0}$  are presented in Figure 9a. It can be observed that  $a_x$  increases with  $v_{z0}$  and reaches the peak value in a relatively shorter time period, which is similar to the behaviour of  $a_z$ (see Figure 3a). Then, the maximal accelerations  $a_{x\max}$  are collected and associated with the initial downward velocity  $v_{z0}$ , as shown in Figure 9b. It is found that  $a_{x\max}$  is a linear function of  $v_{z0}$  itself, which is inconsistent with the law observed in the wedge oblique entry ( $a_{x\max}$  is linearly related to  $v_{z0}^2$  [6]). The reasonable explanation is that the three-dimensional effect and the negative pressure at the rear part weaken the hydrodynamic forces together.

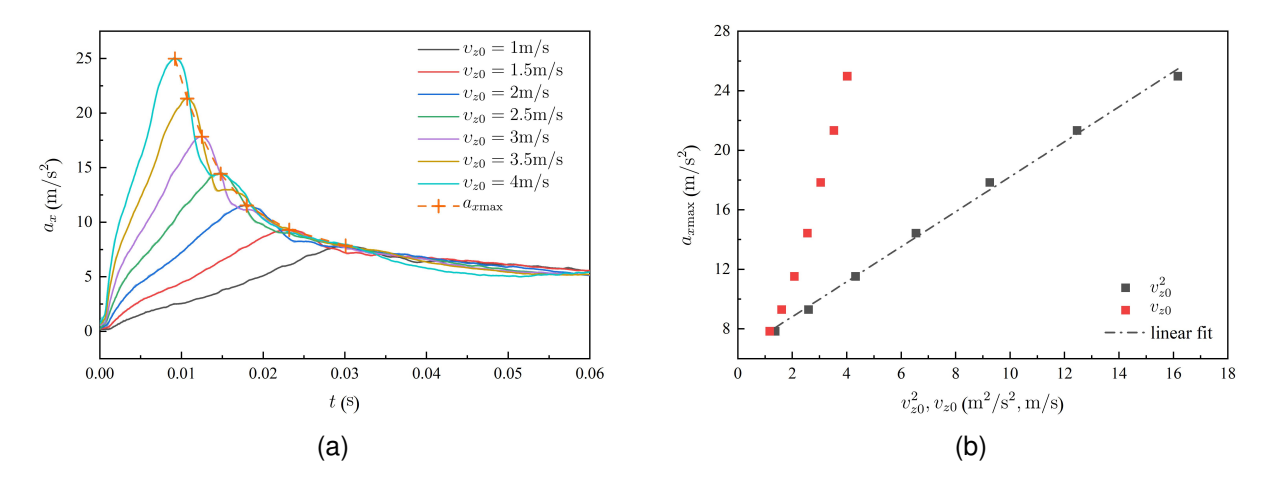


Figure 9 – Effect of initial downward velocity on horizontal acceleration for helicopter ditching with  $\theta_0 = 6^{\circ}$ : (a) time histories of  $a_x$ ; (b) relationship between  $a_{xmax}$  and  $v_{z0}$ .

Besides, comparing the time instants when  $a_{z\max}$  and  $a_{x\max}$  occur, as shown in Figure 10a, it is found that  $a_{x\max}$  appears later than that of  $a_{z\max}$ , and the interval time  $\Delta t^*$  between the two peak values gradually shortens with the increase of  $v_{z0}$ . Combined with Figure 5a and Figure 10b, it can be known that when the horizontal acceleration reaches the maximum value, the attitude angle  $\theta$ , corresponding horizontal velocity  $v_x^*$ , and corresponding penetration depth  $z^*$  for all cases are nearly same, which is consistent with behaviours happened in the case of  $a_{z\max}$ .

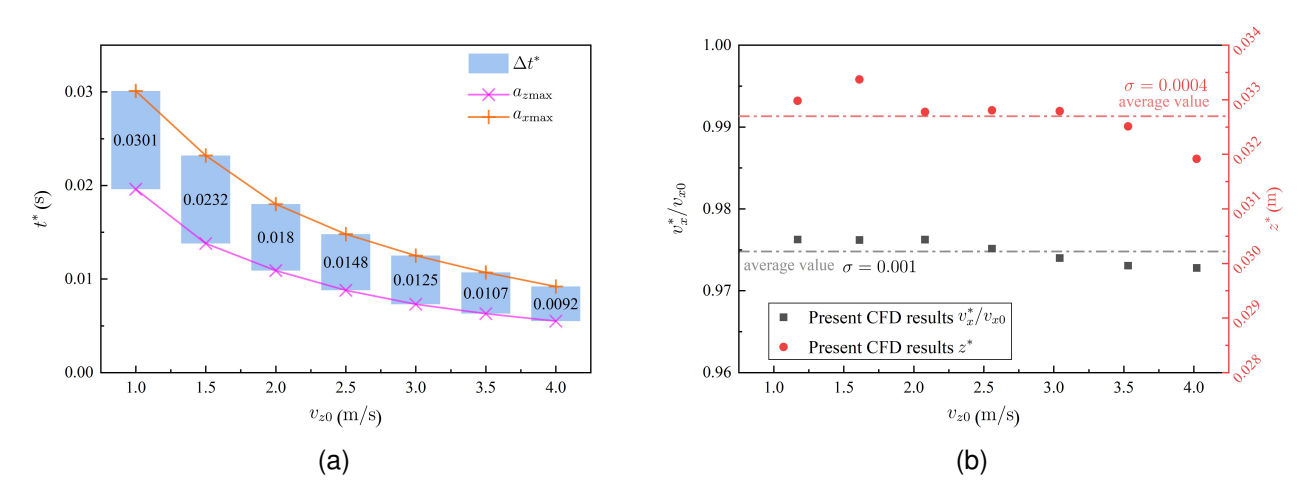


Figure 10 – Effect of initial downward velocity on variable dynamic parameters for helicopter ditching with  $\theta_0 = 6^{\circ}$  when  $a_x$  reaches its maximum: (a)  $\Delta t^*$ ; (b)  $v_x^*$  and  $z^*$ .

# 3.2 Effect of Initial Pitching Angle

When the helicopter attempts to ditching on the water surface with different initial pitching angles, the front and rear angles between the bottom surface of the fuselage and the free surface also change accordingly. Viewed from the longitudinal plane, its initial situation is similar to an asymmetric wedge

water entry problem, as shown in Figure 11. Therefore, the study on the impact of pitching angle on helicopter ditching starts from analyzing the hydrodynamic characteristics of the asymmetric wedge vertical water entry, to explain the effect of pitching angle on the hydrodynamic load. Moreover, in order to mimic the water landing process of the helicopter with different pitching angles as much as possible, an asymmetric wedge is constructed with constant vertex angle, height h and mass M. Only the deadrise angles on both sides of the wedge is changed and the left and right deadrise angles are denoted as  $\beta_L$  and  $\beta_R$ , respectively.



Figure 11 - Relation between helicopter ditching and asymmetric wedge impacting

# 3.2.1 Asymmetric Wedge

Note that only vertical motion is considered for the asymmetric wedge, with an initial vertical velocity of 5.5 m/s and a mass M=4.6842 kg/m [10]. Time histories of  $a_z$  are shown in Figure 12. It can be observed that the larger the difference between  $\beta_L$  and  $\beta_R$ , the higher  $a_{zmax}$ . Particularly, when  $\beta_L$  equals to  $\beta_R$ , the value  $a_{zmax}$  become the smallest one for all cases. It can be further explained through the pressure distribution around the wedge, as shown in Figure 13. Turning to helicopter ditching scenario with different pitching angles, the body with a larger pitching angle could obtain a moderate vertical acceleration to some degree. In practical engineering problems, when pursuing a smaller landing acceleration, the range of pitching angle will also be restricted by other factors, such as pitching moment and the safety distance between the tail wing and the water surface, et al.

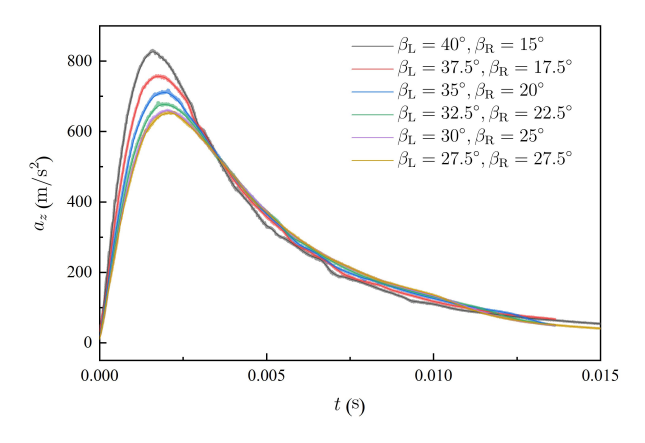


Figure 12 – Effect of deadrise angle  $\beta$  on  $a_z$  for asymmetric wedge impacting

By observing the relationship between  $a_{z\max}$  and deadrise angles on both sides ( $\beta_L$  and  $\beta_R$ ) in Figure 12, and referring to the combined method for symmetric wedge water entry proposed in the work of Lu et al. [10], it is meaningful to extend the combined method to the study of an asymmetric wedge, that is, to quantitatively analyze the relationship among  $a_{z\max}$ ,  $\beta_L$  and  $\beta_R$ . Based on the assumption of the combined method, the definition of added mass mainly depends on the semi-wet width r of the wedge, but for the asymmetric wedge, the wet widths  $r_L$  and  $r_R$  on both sides are not same. According to the concept of the average semi-wet width proposed by Ghadimi et al.[11]:

$$\bar{r} = \frac{1}{2}(r_{\rm L} + r_{\rm R})$$
 (13)

According to the relation of r and z in the case of wedge water entry (see Figure 1), equation (13) can

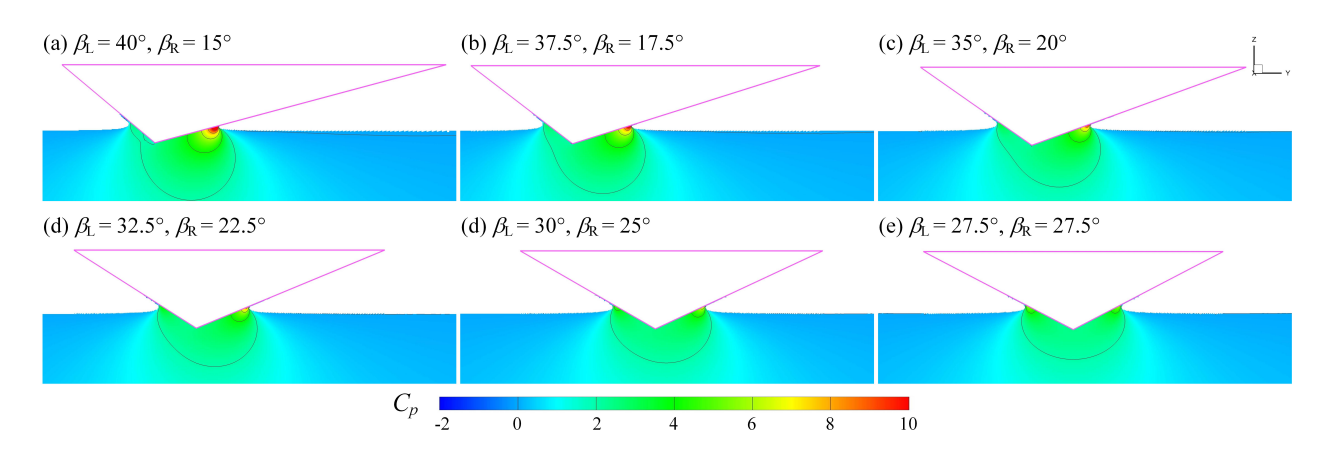


Figure 13 – Pressure distribution for different deadrise angle of asymmetric wedge when  $a_z$  reaches its maximum

be rewritten as:

$$\frac{z}{\tan \bar{\beta}} = \frac{1}{2} \left( \frac{z}{\tan \beta_{\rm L}} + \frac{z}{\tan \beta_{\rm R}} \right) \tag{14}$$

where  $\bar{\beta}$  represents the average deadrise angle. Removing the parameter z, it can be expressed as:

$$\tan \bar{\beta} = \frac{2 \cdot \tan \beta_{L} \cdot \tan \beta_{R}}{\tan \beta_{L} + \tan \beta_{R}}$$
 (15)

At this point, considering both the influence of  $\beta_L$  and  $\beta_R$ , equation (15) provides a new quantitative relationship to unify the two different deadrise angles. For  $\beta_L$  and  $\beta_R$  respectively, according to Dobrovol'skaya's theoretical solution [12, 13], the relationship between  $\gamma$  and deadrise angle  $\beta$  in Figure 14a is obtained, while it is difficult to obtain an effective pile-up coefficient for the asymmetric wedge. Referring to the theoretical formula of the pile-up coefficient mentioned in the work of Lu et al. [10], and substituting the average deadrise angle  $\bar{\beta}$ , the average pile-up coefficient  $\bar{\gamma}$  is obtained as follow:

$$\bar{\gamma} = \frac{a_{z\text{max}}}{v_{z0}^2 \left(\frac{5}{6}\right)^3 \sqrt{\frac{2\pi\rho}{5M}}} \cdot \tan(\bar{\beta})$$
 (16)

By substituting the peak acceleration values obtained from present CFD results (see in Figure 12) into equation (16), the relationship between  $\bar{\gamma}$  and  $\bar{\beta}$  that can be used for the water entry of the asymmetric wedge is obtained, as shown in Figure 14b. The fitting relationship is obtained as  $\bar{\gamma}$  =  $-0.3245 \tan(\bar{\beta}) + 1.3841$ , similar to the behaviour observed on symmetric wedge water entry condition described in [10]. Similarly, the expression for  $a_{zmax}$  for the asymmetric wedge can be derived, as well as  $z^*$ ,  $v_z^*$ , and  $t^*$ :

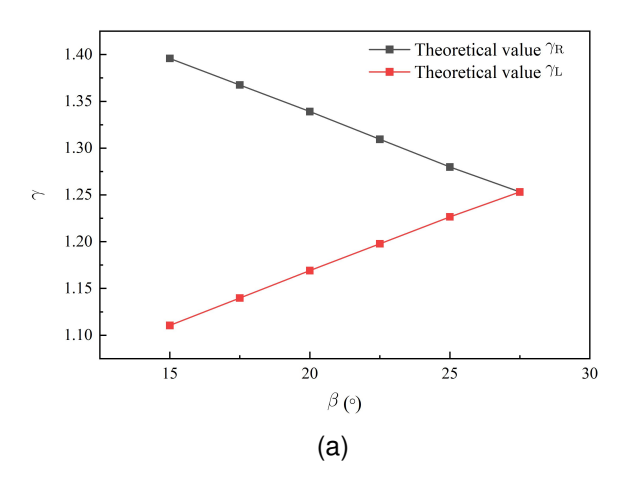
$$a_{z\max} = v_{z0}^2 \left(\frac{5}{6}\right)^3 \frac{\bar{\gamma}}{\tan(\bar{\beta})} \sqrt{\frac{2\pi\rho}{5M}}$$

$$z^* = \sqrt{\frac{2M}{5\pi\rho\bar{\gamma}^2}} \tan(\bar{\beta})$$
(17a)

$$z^* = \sqrt{\frac{2M}{5\pi\rho\bar{\gamma}^2}}\tan(\bar{\beta})$$
 (17b)

$$v_z^* = \frac{5}{6}v_{z0} \tag{17c}$$

$$t^* = \frac{1}{v_{z0}} \frac{16}{15} \sqrt{\frac{2M}{5\pi\rho\bar{\gamma}^2}} \tan(\bar{\beta})$$
 (17d)



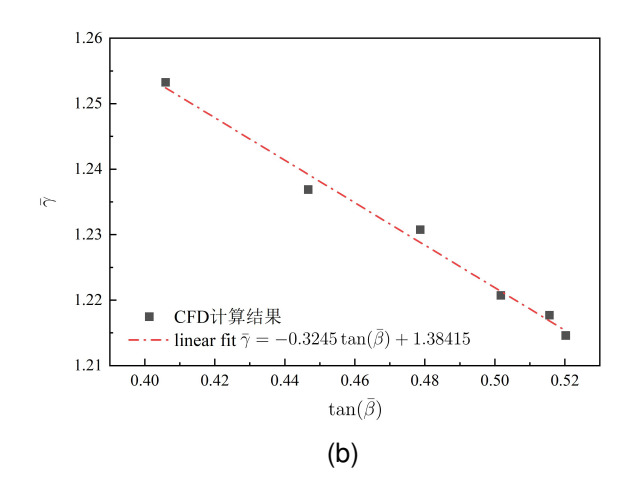


Figure 14 – Relationship between average pile-up coefficient  $\bar{\gamma}$  and average deadrise angle  $\bar{\beta}$  for asymmetric wedge: (a)  $\gamma$  and  $\beta$ ; (b)  $\bar{\gamma}$  and  $\bar{\beta}$ 

Figure 15 shows the effect of average deadrise angle  $\bar{\beta}$  on the maximal vertical acceleration  $a_{z\max}$  and the corresponding parameter, such as the penetration depth  $z^*$ , velocity  $v_z^*$ , and time  $t^*$ . As can be seen from Figure 15a,  $a_{z\max}$  is a linear function of  $\bar{\beta}$ , and the numerical results are highly consistent with the theoretical estimates. Note that the average pile-up coefficient  $\bar{\gamma}$  in the theoretical estimates is obtained by the fitting relationship  $\bar{\gamma}=-0.3245\tan(\bar{\beta})+1.38415$  in Figure 14b. In Figure 15b, the numerical results of  $\kappa$  float around the theoretical value 5/6 with the root mean square error (RMSE) 0.004. The numerical results of  $t^*$  and  $z^*$  also fluctuate near the theoretical solution. It can be concluded that the validity and accuracy of the proposed theoretical equation (17) for the asymmetric wedge are sufficient.

# 3.2.2 Helicopter

Based on the above research on the hydrodynamic characteristics of the helicopter ditching on still water with different initial downward velocity and the asymmetric wedge water entry with different deadrise angle, the effect of the initial pitching angle  $\theta_0$  on the ditching performance of the helicopter with different initial downward velocity  $v_{z0}$  is fully discussed, as shown in Figure 16. It can be found in Figure 16a that for different cases of  $\theta_0$ ,  $a_{zmax}$  still maintains a linear quantitative relationship with  $v_{z0}^2$ , and the slope value of the linearity reduces with the increase of  $\theta_0$ . Specifically, under the same value of  $v_{z0}$ , a relatively larger  $\theta_0$  can obtain a smaller  $a_{zmax}$ , which is consistent with the phenomenon observed in the asymmetric wedge case. Since  $a_{zmax}$  varies with  $\theta_0$ , the time history of acceleration changes accordingly, meaning that the time integral term of acceleration (water entry velocity) changes. It can be used to explain the fluctuation behaviour of  $\kappa$  in Figure 16b.

Taking  $v_{z0}$ =2 m/s as an example case, the influence of  $\theta_0$  on the angular acceleration  $\dot{\omega}_y$  and horizontal acceleration  $a_x$  of the helicopter during the water landing process is further analyzed, as shown in Figure 17a and b. A more gentle variation in  $\dot{\omega}_y$  can be observed with a relatively larger  $\theta_0$  while the tendency of  $a_x$  is quite different. This also shows that in practical engineering problems, it is necessary to consider the influence of the initial pitching angle on the vertical and horizontal accelerations comprehensively, and the initial pitching angle should be as large as possible within a reasonable range [8].

Figure 18 shows the comparison of the numerical results and theoretical solutions of  $t^*$  and  $z^*$  during the water landing process of the helicopter with different initial pitching angle  $\theta_0$ . As it can be seen,  $t^*$  is still a linear function of  $1/v_{z0}$ , and  $z^*$  also shows a trend of approaching a constant value. Referring to the theoretical relationship mentioned in Section 2.1and Figure 16a, the fitting relationships of  $a_{zmax}$  in terms of  $v_{z0}^2$  with shape factors  $S(\gamma, \beta, M)$  are listed in Table 2. An increasing trend can be found on  $S(\gamma, \beta, M)$  with the increase of initial pitching angle, indicating that function of shape factor.

Using the theoretical expression of  $t^*$  (see equation (4)), the theoretical results of  $t^*$  are obtained. Compared with the numerical results in Figure 18a, the three-dimension factor  $\mu_{3D}$  could be figured

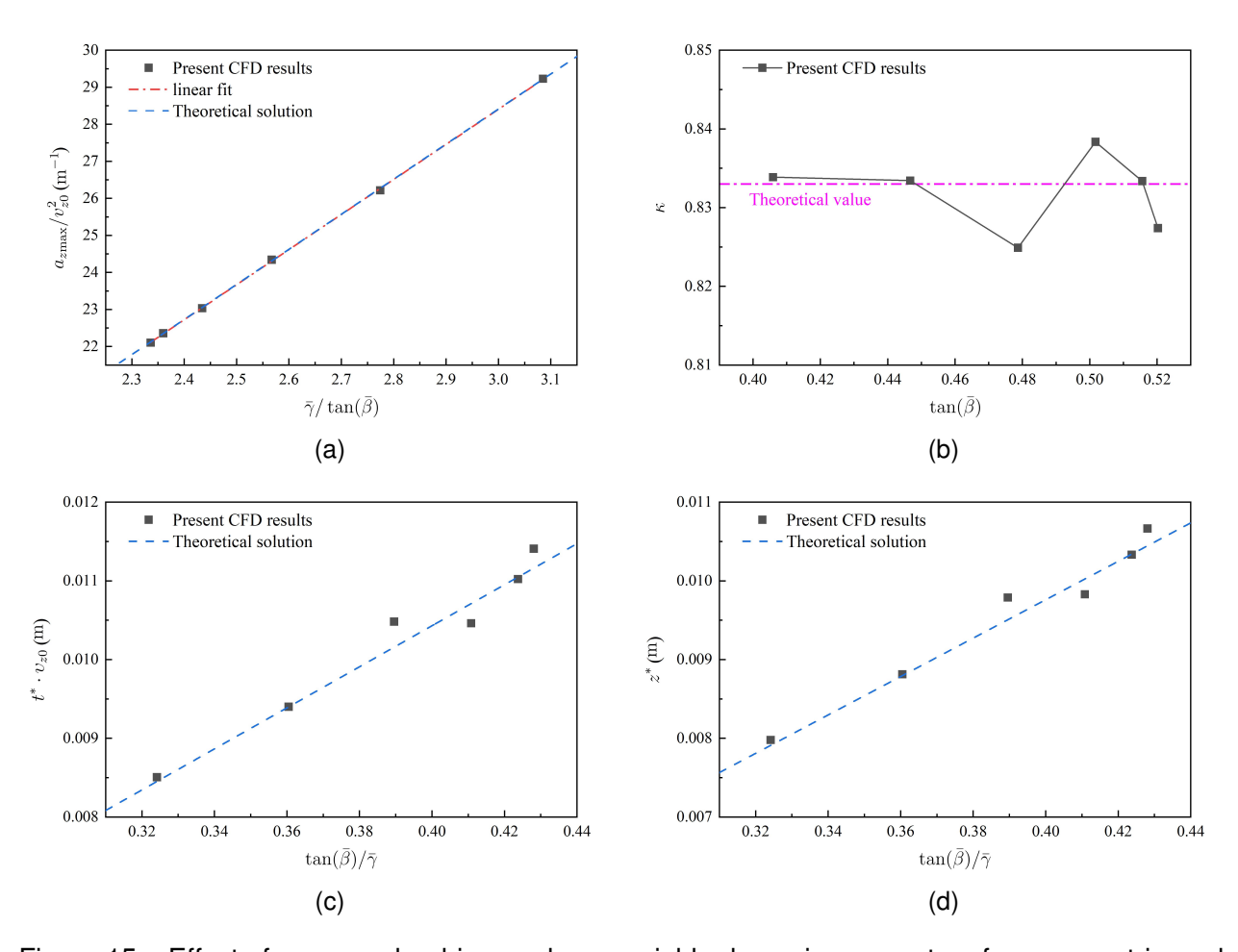


Figure 15 – Effect of average deadrise angle on variable dynamic parameters for asymmetric wedge impacting: (a)  $a_{zmax}$ ; (b)  $\kappa$ ; (c)  $t^*$ ; (d)  $z^*$ .

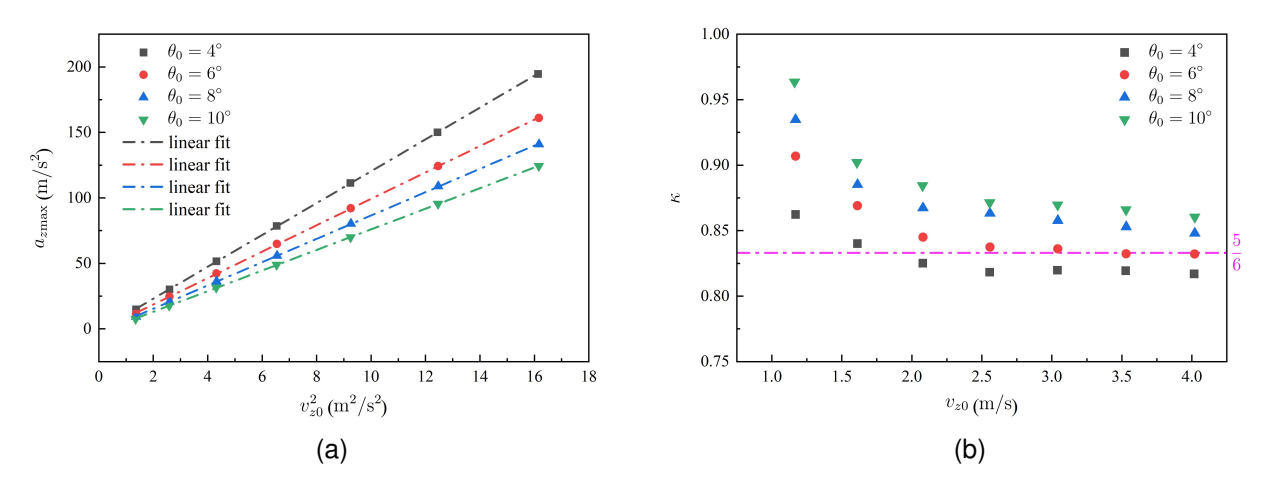


Figure 16 – Effect of  $\theta_0$  and  $v_{z0}$  on acceleration for helicopter ditching: (a)  $a_{zmax}$ ; (b)  $\kappa$ .

Table 2 – Comparison of theoretical results for helicopter ditching with different  $\theta_0$ .

$\theta_0$	fitting formula $a_{zmax}$	$S(\gamma,\beta,M)$	$\mu_{\mathrm{3D}}$	z*theory	RMSE of $z_{\text{theory}}^*$
4°	$a_{z\max} = 12.1638v_{z0}^2 - 1.2997$	2.8392	1.0276	0.0195	0.0023
$6^{\circ}$	$a_{z\max} = 10.0841v_{z0}^2 - 1.5655$	4.1311	0.9442	0.0216	0.0008
$8^{\circ}$	$a_{z\max} = 8.8999v_{z0}^{2} - 2.4341$	5.3036	0.8957	0.0233	0.0014
$10^{\circ}$	$a_{z\max} = 7.8668v_{z0}^2 - 2.6908$	6.7880	0.8169	0.0240	0.0007

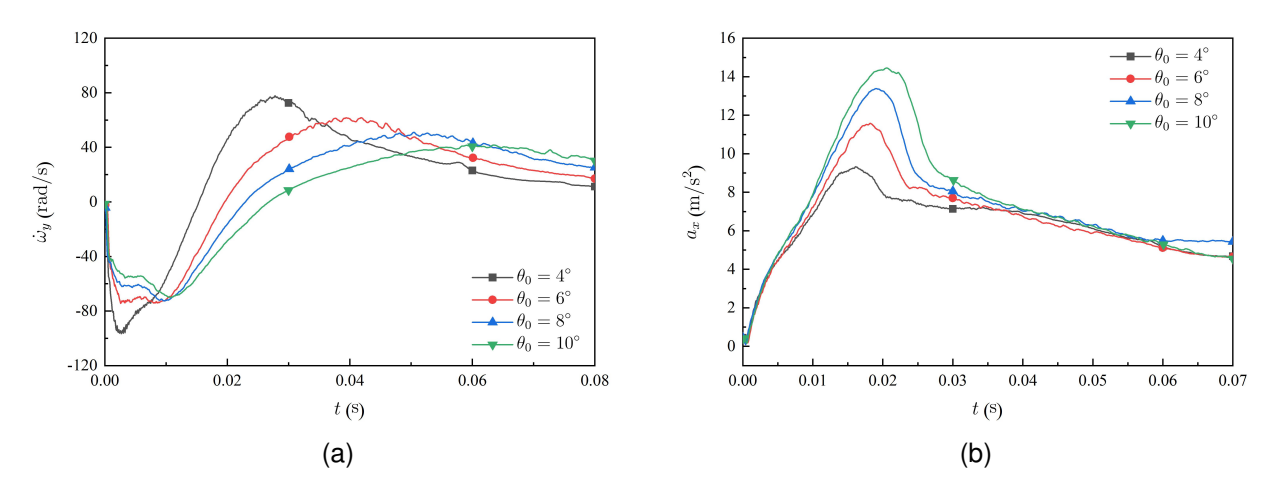


Figure 17 – Effect of  $\theta_0$  in the case of  $v_{z0}$ =2 m/s: (a)  $\dot{\omega}_v$ ; (b) $a_x$ .

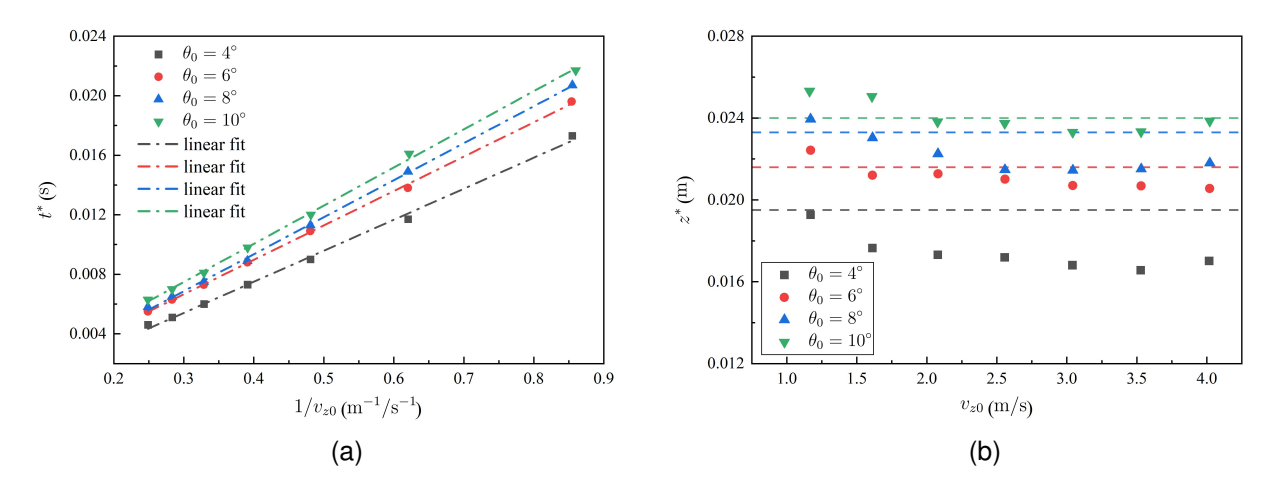


Figure 18 – Comparison of theoretical solutions and numerical results: (a) $t^*$ ; (b)  $z^*$ .

out, as presented in Table 2. Subsequently, the theoretical values of  $z^*$  are gained. Based on the comparison of numerical and theoretical values, it is found that the root mean square error (RMSE) of  $z^*$  is very small, indicating that the theoretical solution has a high prediction accuracy.

## 4. Conclusion

In order to evaluate the effect of initial downward velocity and pitching angle on hydrodynamic behavior during helicopter ditching event, a large amount of cases has been carried out to analyze through solving the URANS equations coupled with VOF method. Results can be drawn as:

- I. The impact of initial downward velocity on ditching performance is analysed numerically and theoretically with a shape factor. The factor is then utilized to analyze the corresponding time, velocity, and penetration depth when the peak acceleration occur. The theoretical predictions closely match the numerical results, with an error of less than 10%.
- II. In examining the influence of initial pitching angle on helicopter ditching performance, an asymmetric wedge is employed to explain the role of the initial pitching angle. Additionally, the average deadrise angle is introduced to extend the theoretical model, derived from the symmetric wedge to asymmetric situation.

## 5. Contact Author Email Address

Mail to: loux27@163.com

# 6. Acknowledgments

This work has been supported by the Aeronautical Science Foundation of China (No. 20220023052001 and No. 20230023052001) and Postgraduate Research & Practice Innovation Program of Jiangsu Province(No.SJCX24 0123).

# 7. Copyright Statement

The authors confirm that they hold copyright on all of the original material included in this paper. The authors also confirm that they have obtained permission, from the copyright holder of any third party material included in this paper, to publish it as part of their paper. The authors confirm that they give permission, or have obtained permission from the copyright holder of this paper, for the publication and distribution of this paper as part of the ICAS proceedings or as individual off-prints from the proceedings.

## References

- [1] Hughes K, Vignjevic R, Campbell J, Vuyst T D, Djordjevic N, and Papagiannis L. From aerospace to offshore: bridging the numerical simulation gaps-simulation advancements for fluid structure interaction problems. *International Journal of Impact Engineering*, 61:48–63, 2013.
- [2] McBride E E and Fisher L J. Experimental investigation of the effect of rear-fuselage shape on ditching behavior. Technical Report NACA TN 2929, NACA, Washington, D. C., 1953.
- [3] Qu Q, Hu M, Guo H, Liu P, and Agarwal R K. Study of ditching characteristic of transport aircraft by global moving mesh method. *Journal of Aircraft*, 52(5):1550–1558, 2015.
- [4] Guo B, Liu P, Qu Q, and Wang J. Effect of pitch angle on initial stage of a transport airplane ditching. *Chinese Journal of Aeronautics*, 26(1):17–26, 2013.
- [5] Cheng H, Ming F R, Sun P N, Wang P P, and Zhang A M. Towards the modeling of the ditching of a ground-effect wing ship within the framework of the sph method. *Applied Ocean Research*, 82:370–384, 2019.
- [6] Lu Y, Del Buono A, Xiao T, Iafrati A, Deng S, and Xu J. On applicability of von karman's momentum theory in predicting the water entry load of v-shaped structures with varying initial velocity. *Ocean Engineering*, 262:112249, 2022.
- [7] Hirt C W and Nichols B D. Volume of fluid (vof) method for the dynamics of free boundaries. *Journal of Computational Physics*, 39(1):201–225, 1981.
- [8] T Xiao, Y Lu, S Deng, H Zhi, Z Zhu, and J Chen. Hydrodynamic characteristics of a helicopter ditching on different positions of wavy water. *Journal of Aircraft*, 58(5):1–12, 2021.
- [9] Iafrati A. Experimental investigation of the water entry of a rectangular plate at high horizontal velocity. *Journal of Fluid Mechanics*, 799:637–672, 2016.
- [10] Lu Y, Del Buono A, Xiao T, Iafrati A, Xu J, Deng S, and Chen J. Parametric study on the water impacting of a free-falling symmetric wedge based on the extended von karman's momentum theory. *Ocean Engineering*, 271:113773, 2023.
- [11] Ghadimi P, Tavakoli S, Dashtimanesh A, and Taghikhani P. Dynamic response of a wedge through asymmetric free fall in 2 degrees of freedom. *Proceedings of the Institution of Mechanical Engineers, Part M: Journal of Engineering for the Maritime Environment*, 233(1):229–250, 2019.
- [12] Dobrovol'skaya Z N. On some problems of similarity flow of fluids with a free surface. *Journal of Fluid Mechanics*, 36(4):805–829, 1969.
- [13] Zhao R and Faltinsen O M. Water entry of two-dimensional bodies. *Journal of Fluid Mechanics*, 246:593–612, 1993.